# optica

# Highly efficient scalable monolithic semiconductor terahertz pulse source: supplementary material

**J. A. Fülöp,**[1,2,3,*] **Gy. Polónyi,**[1,2] **B. Monoszlai,**[2,3] **G. Andriukaitis,**[4]
**T. Balciunas,**[4] **A. Pugzlys,**[4,5] **G. Arthur,**[6] **A. Baltuska,**[4,5] **and J. Hebling**[1,2]

[1]*MTA-PTE High-Field Terahertz Research Group, Pécs, Hungary*
[2]*Institute of Physics & Szentágothai Research Centre, University of Pécs, Pécs, Hungary*
[3]*ELI-ALPS, ELI-Hu Nkft., Szeged, Hungary*
[4]*Photonics Institute, Vienna University of Technology, Vienna, Austria*
[5]*Center for Physical Sciences & Technology, Vilnius, Lithuania*
[6]*Scitech Precision Ltd., Oxford, United Kingdom*
*\*Corresponding author: fulop@fizika.ttk.pte.hu*

## 1. CHARACTERIZATION OF THE CONTACT-GRATING THZ SOURCE

The proper orientation of the grating lines with respect to the dielectric *Z*-axis of the (110)-oriented ZnTe crystal substrate was essential for efficient THz generation. The dependence of the second-order nonlinear polarization on the angle between the *Z*-axis and the pump polarization direction [$\varphi$, see main article, Fig. 1(b)] can be calculated as $|P|^2(\varphi) \propto \sin^2(\varphi)\left[4 - 3\sin^2(\varphi)\right]$ (Ref. [1]). It follows that the highest THz generation efficiency can be expected at $\varphi = 54.7°$ and $125.3°$. The intensity of a second-harmonic (SH) beam exhibits the same dependence on the polarization angle [Fig. S1(a)]. Therefore, we used SH generation, pumped at a fundamental wavelength of 1030 nm, to characterize the domain structure and orient the ZnTe substrate prior to grating manufacturing. The inset in Fig. S1(a) shows a CCD camera image of the SH signal from the $20\times20$ mm$^2$ substrate, clearly indicating multiple crystal domains with different orientations. The $10\times10$ mm$^2$ contact grating (CG) was positioned to lay entirely inside the largest domain. The direction of the grating lines can be chosen along $\varphi = 54.7°$ or $125.3°$, corresponding to one of the two maxima and taking into account that the diffraction efficiency is highest for a TE-polarized pump beam [2]. The THz signal measured as function of the pump polarization angle is shown in Fig. S1(b). The asymmetry is caused by the difference in diffraction efficiencies for the TE (parallel to grating lines) and TM (perpendicular to grating lines) pump polarization directions.

A careful characterization of the grating structures was carried out by using optical, scanning electron (SEM), and atomic force microscopy (AFM). As mentioned in the main article, bubbles in the substrate, uncovered as pits in the polished surface [Fig. S2(a)], resulted in the disruption of the resist film during manufacturing and caused defects of grating lines. These are clearly seen as light yellow lines, starting from pits, in the AFM micrograph in Fig. S2(b). Such defects can be suppressed by using ZnTe or other semiconductor substrates of better quality.

## 2. PUMP SOURCE

The pump source was a supercontinuum-seeded four-stage optical parametric amplifier (OPA) system, delivering 144 fs pulses at 1.7 μm wavelength with 50 Hz repetition rate (Fig. S3). The pulses were characterized by SH generation frequency-resolved optical gating (SHG FROG). The measured temporal and spectral intensities and phases are shown in Fig. S3. Up to 3.2 mJ pulse energy was used to pump the ZnTe CG. The OPA was driven by a cryogenically cooled Yb:CaF$_2$ chirped-pulse amplification laser system consisting of an oscillator, a regenerative amplifier, and a multipass power amplifier, operating at 1.03 μm wavelength and delivering 200 fs pulses with 90 mJ energy at 50 Hz repetition rate [3].

## 3. SIMULATION OF THZ GENERATION

For the simulation of THz generation, the one-dimensional wave equation with the nonlinear polarization was solved in the spectral domain [4]. The THz waveform was obtained by Fourier transformation. The model takes into account the variation of the pump pulse duration with propagation distance due to material and angular dispersions, the non-collinear propagation of pump and

THz beams, and the absorption in the THz range due to phonon resonances. Optical refractive indices for ZnTe were taken from Ref. [5], and for GaP from Ref. [6]. THz refractive indices for ZnTe were taken from Ref. [7,8], and for GaP from Ref. [9].
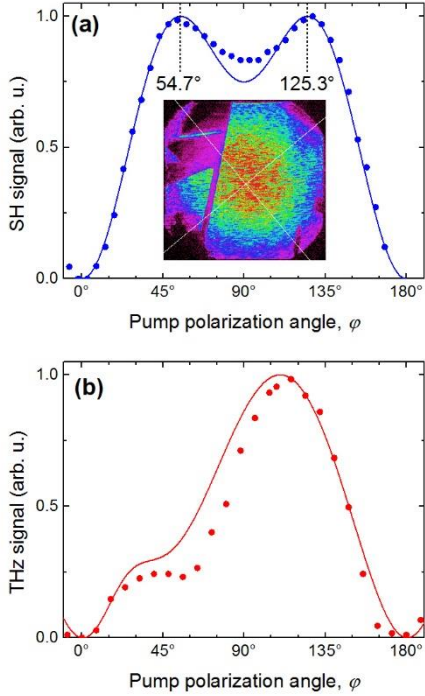


Fig. S1. (a) Measured (symbols) and calculated (solid line) SH intensity as function of the pump polarization angle $\varphi$, measured from the $Z$-axis of ZnTe. The inset shows the SH intensity recorded with a CCD camera. (b) Measured (symbols) and calculated (solid line) THz signal as function of the pump polarization angle.
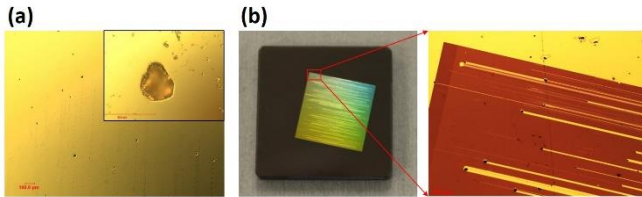


Fig. S2. (a) Optical microscope image of the surface of the ZnTe substrate. The inset shows a pit in the surface at a larger magnification. (b) Photograph of the CG (left panel) and AFM micrograph of part of the CG surface (right panel).

The choice of the semiconductor nonlinear material and the phase matching frequency are very important for the design of a CG THz source. The achievable THz generation efficiency and peak electric field sensitively depend on this choice, as shown by simulation results for ZnTe and GaP (see Fig. 5 in the main article). For phase matching at 1 THz in ZnTe, the efficiency is predicted to increase monotonically over the investigated 8.8 mm crystal length [red and blue solid lines in Fig. 5(a) in the main article]. In contrast, phase matching at 2 THz causes the saturation of efficiency after a short distance [about 2.6 mm at room temperature, and 3.5 mm at cryogenic temperature; red and blue dashed lines in Fig. 5(a) in the main article, respectively]. The peak electric field exhibits similar behavior [Fig. 5(c) in the main article]. About 1.5× higher peak field is predicted for phase matching at 1 THz than for 2 THz [Fig. S4(a)], despite the lower frequency in the former case. This behavior can be attributed mainly to the effect of an absorption peak at 1.7 THz

in ZnTe, with a peak room temperature absorption coefficient of about 11.7 cm$^{-1}$ [Fig. S4(b)].
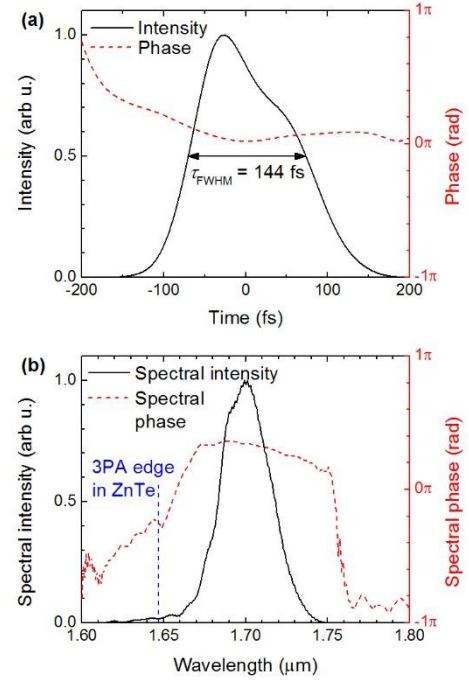


Fig. S3. Reconstructed intensity and phase of the pump pulses in the temporal (a) and spectral (b) domains from SHG FROG measurement. The vertical dashed blue line in (b) indicates the wavelength above which no three-photon absorption (3PA) is present in ZnTe.

Phase matching at 1 THz in ZnTe enables efficient generation of THz spectral components up to about 1.2 THz [Fig. S4(c), se also red solid line in Fig. 5(b) in the main article], which is below the absorption peak. The small absorption coefficient ($\alpha \lesssim 5$ cm$^{-1}$) in this region enables a long effective interaction length. In contrast, phase matching above the absorption peak suppresses low-frequency spectral components. A narrow spectrum is being formed, centered at the phase matching frequency [2 THz in case of Fig. S4(d) and the blue dashed line in Fig. 5(b) in the main article]. The high absorption ($\alpha \gtrsim 8$ cm$^{-1}$) in this spectral range limits the effective interaction length and causes the saturation of the efficiency. Cooling the crystal may result in higher efficiency and field strength (Fig. 5 in the main article), but it does not eliminate the saturation at higher frequencies.

The CG technique can easily be adopted to other semiconductor nonlinear materials. GaP can also be pumped at 1.7 μm to suppress two- and three-photon pump absorption. The effective nonlinear coefficient of this material is 24.8 pm/V [10,11], almost three times smaller than that of ZnTe. However, the absorption coefficient and the refractive index dispersion of GaP are much smaller [Fig. S5(a)]. This feature enables in GaP a more favorable scaling of the efficiency and the peak electric field with the interaction length even at higher frequencies. For example, both efficiency and peak field are predicted to increase monotonically over the investigated 9.3 mm crystal length for phase matching at 2 THz [see Figs. 5(a) and 5(b) in the main article]. The corresponding evolution of the THz spectrum is shown in Fig. S5(b). A broadband spectrum extending up to 3 THz can be generated even for large crystal lengths of 9.3 mm, in contrast to the narrow-peaked spectrum in ZnTe [Fig. S4(d)]. Accordingly, a significantly higher peak electric field is predicted in GaP [black dashed line in Fig. S4(a)].
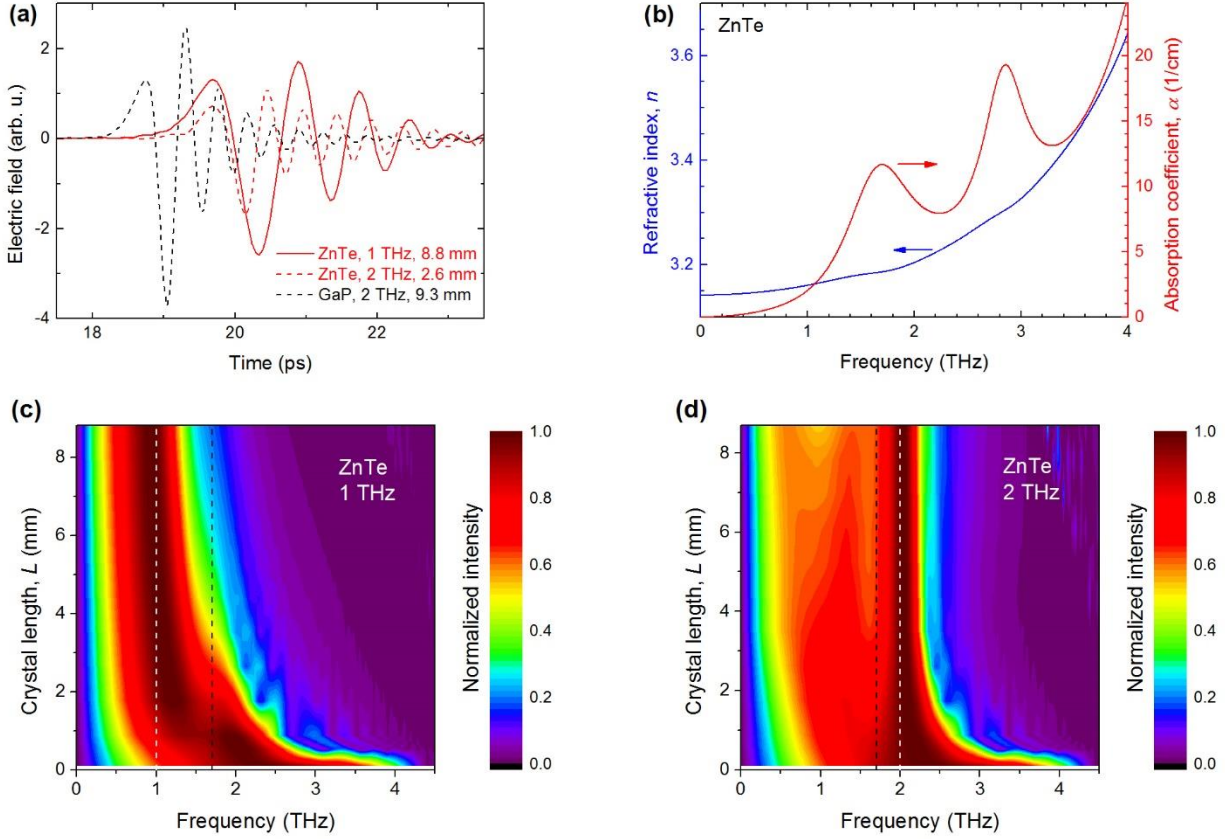
Fig. S4. Simulation results for ZnTe. (a) THz waveforms for 1 THz (red solid line) and 2 THz (red dashed line) phase matching frequencies in ZnTe. The crystal lengths are 8.8 mm and 2.6 mm, respectively. Latter corresponds to the predicted maximum of the peak field (see also Fig. 5c in the main article). For sake of simplicity, the waveform for GaP is also included here for phase matching at 2 THz and 9.3 mm crystal length. (b) Refractive index and absorption coefficient of ZnTe in the THz range [7,8]. Variation of the THz spectrum with crystal length in ZnTe for 1 THz (c) and 2 THz (d) phase matching frequencies, indicated by the white dashed lines. The black dashed lines indicate the absorption peak at 1.7 THz. In all cases, the crystal was at room temperature and a pump pulse duration of 144 fs was assumed.
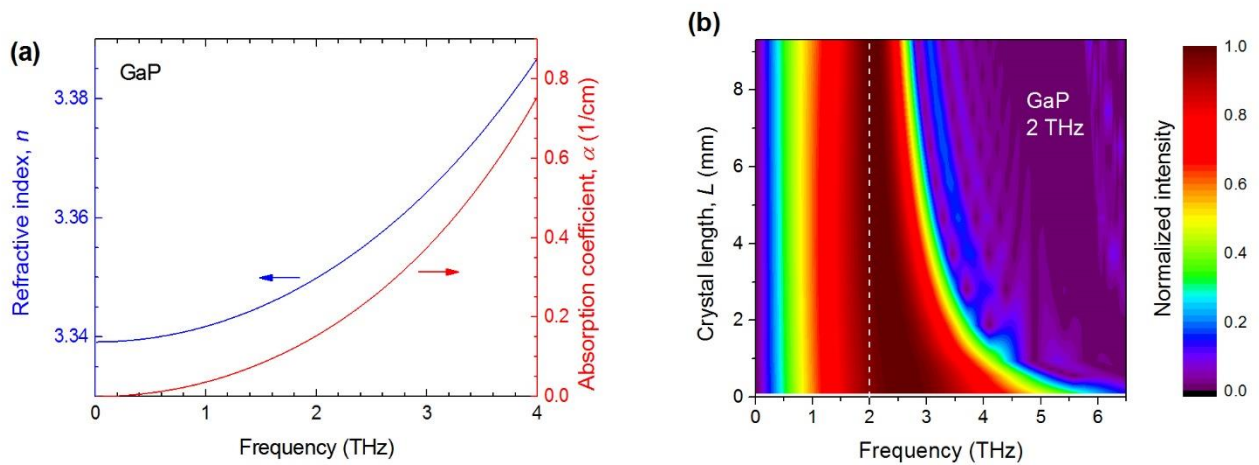


Fig. S5. (a) Refractive index and absorption coefficient for GaP [9]. (b) Calculated variation of the THz spectrum with crystal length in GaP for 2 THz phase matching frequency, indicated by the white dashed line. The crystal was at room temperature and a pump pulse duration of 144 fs was assumed.

# REFERENCES

1. A. Rice, Y. Jin, X. F. Ma, X.-C. Zhang, D. Bliss, J. Larkin, and M. Alexander, "Terahertz optical rectification from <110> zinc-blende crystals," Appl. Phys. Lett. **64,** 1324–1326 (1994)

2. Z. Ollmann, J.A. Fülöp, J. Hebling, and G. Almási, "Design of a high-energy terahertz pulse source based on ZnTe contact grating," Opt. Commun. **315,** 159–163 (2014)

3. G. Andriukaitis, E. Kaksis, G. Polónyi, J. A. Fülöp, A. Baltuška, A. Pugžlys, "220-fs 110-mJ Yb:CaF2 cryogenic multipass amplifier," in CLEO: 2015, OSA Technical Digest (online) (Optical Society of America, 2015), paper SM1P.7

4. J. A. Fülöp, L. Pálfalvi, G. Almási, and J. Hebling, "Design of high-energy terahertz sources based on optical rectification," Opt. Express **18,** 12311–12327 (2010)

5. H. H. Li, "Refractive index of ZnS, ZnSe, and ZnTe and its wavelength and temperature derivatives," J. Phys. Chem. Ref. Data **13,** 103–150 (1984)

6. W. L. Bond, "Measurement of the refractive indices of several crystals," J. Appl. Phys. **36,** 1674–1677 (1965)

7. M. Schall, M. Walther, and P. Uhd Jepsen, "Fundamental and second-order phonon processes in CdTe and ZnTe," Phys. Rev. B **64,** 094301 (2001)

8. K. Wynne and J. J. Carey, "An integrated description of terahertz generation through optical rectification, charge transfer, and current surge," Opt. Commun. **256,** 400–413 (2005)

9. D. F. Parsons and P. D. Coleman, "Far infrared optical constants of Gallium Phosphide," Appl. Opt. **10,** 1683–1685 (1971)

10. J. Hebling, K.-L. Yeh, M. C. Hoffmann, B. Bartal, and K. A. Nelson, "Generation of high-power terahertz pulses by tilted-pulse-front excitation and their application possibilities," J. Opt. Soc. Am. B **25,** B6–B19 (2008)

11. D. F. Nelson and E. H. Turner, "Electro-optic and piezoelectric coefficients and refractive index of gallium phosphide," J. Appl. Phys. **39,** 3337–3343 (1968)